

Article

Fabrication of Composite Ultrafiltration Membrane by Coating Urea Formaldehyde Resin on Filter Paper

Hailong Lu ^{1,2}, Lili Zhang ¹, Yong Shi ¹, Jinxia Ma ¹ and Xiaofan Zhou ^{1,2,*}

¹ Jiangsu Co-Innovation Center of Efficient Processing and Utilization of Forest Resources, Nanjing Forestry University, Nanjing 210037, China; hailonglull@126.com (H.L.); zhangll@njfu.edu.cn (L.Z.); shiyong@hotmail.com.cn (Y.S.); jxma@njfu.edu.cn (J.M.)

² National-Provincial Joint Engineering Research Center of Electromechanical Product Packaging, Nanjing Forestry University, Nanjing 210037, China

* Correspondence: zxiaofan@njfu.com.cn; Tel.: +86-25-85428932

Received: 23 February 2020; Accepted: 14 May 2020; Published: 18 May 2020



Abstract: Urea-formaldehyde resin (UFR), a thermosetting resin, is used to prepare ultrafiltration membranes because of its excellent mechanical properties and filtration performance. Herein, a porous ultrafiltration membrane is prepared by coating a mixture of UFR and carboxymethylcellulose (CMC) on the surface of filter paper via a facile acid-curing treatment method. CMC is used as a thickening agent, and hydrochloric acid is used as a curing agent to accelerate composite membrane formation. The mesoporous UFR is embedded in the large pores of the paper matrix by coating treatment, and the presence of CMC can decrease the flowability of the resin. The effects of UFR concentration, CMC dosage, and hydrochloric acid concentration on the performance of the composite ultrafiltration membrane are studied. The ultrafiltration membrane demonstrates a rejection rate of 85% and a pure water flux of 850 L/(m²·h) with the optimized resin concentration, CMC dosage, hydrochloric acid concentration, and coating amount at 30%, 20% (resin dry), 12%, and 250 g/m², respectively.

Keywords: urea-formaldehyde resin; ultrafiltration membrane; rejection rate; pure water flux

1. Introduction

Ultrafiltration membranes have been extensively applied in water treatment to remove bacteria and macromolecules, colloidal materials, oil droplets, and suspended solids (SS), etc. [1–5]. Ultrafiltration membranes have a pore size of 2–100 nm, corresponding to a molecular weight cutoff of 1000–500,000 Da in the operating pressure range of 0.1–1.0 MPa [6,7]. The phase inversion process is an effective method for producing polymer ultrafiltration (UF) membranes. There are four phase inversion processes: thermally induced phase separation [8], immersion precipitation [9], dry-casting of a polymer solution [10], and vapor-induced phase separation [11]. However, polymeric ultrafiltration membranes are prone to fouling during long-term operation because of their intrinsic hydrophobicity and low hydrophilicity. Membrane fouling, caused by the adsorption and accumulation of contaminants on the external surface and within the channels of the membrane, not only results in channel blockage and reduces permeate flux, but also significantly shortens the membrane lifespan. It has been widely acknowledged that membranes with high hydrophilicity are less susceptible to fouling.

Thermoplastic polymers, such as polyvinyl chloride [12,13], polyamide [14,15], cellulose acetate [16,17], and others [18–21], are widely used as membrane separation materials. However, thermoplastic polymer membranes are subject to a high degree of fouling, so it is imperative to improve their hydrophilicity [22–25]. Water-soluble resins are more hydrophilic than thermoplastic polymers. UFR, a water-soluble thermosetting resin, has received extensive

attention because of its hydrophilicity, decent mechanical strength, superior physical and chemical stabilities, and low cost [26–30]. Thermosetting UFR has very good compressive strength, so the prepared membrane material can have strong compressive strength. The membrane can be used in high-operating-pressure conditions because of its good filtering speed. Thermosetting resins have higher temperature resistance than conventional thermoplastic resins, enabling stable ultrafiltration at higher temperatures. However, high temperatures have a negative effect on the performance of thermosetting membranes during preparation process. High temperatures are unfavorable for the porosity ratio of the membrane as the water content is decreased, which leads to a low porosity ratio.

In general, toxic reagents such as N,N-dimethylformamide (DMF) and N-methylpyrrolidone are used in membrane production [31–34]. Although the excellent properties of polymer membranes in various applications have been widely recognized, they result in environment issues during the production and disposal stages of their life cycle. The sustainability of thin membranes can be further improved by replacing the present non-renewable polymeric materials from petrochemical resources with naturally occurring polymers like cellulose [35–39]. Cellulose, as the most common organic polymer in the world, has the potential to reduce environmental pressure [40–43]. For instance, Varanasi et al. [32] reported that cellulose nanofiber composite ultrafiltration membranes are readily recyclable as a feed stock for the conventional papermaking process. Wang et al. [44] proposed a method to prepare paper-based ultrafiltration membranes via paper coating technology.

In this project, water-soluble UFR was used as a precursor; a UFR solution was gelation-cured by adding an appropriate amount of acid. By controlling the process conditions of gel curing, a UFR-based ultrafiltration membrane with a three-dimensional network structure was successfully prepared. In this project, the thickener plays an important role in making the porosity of the membrane uniform in the system. The mechanism of UFR gel curing was analyzed and discussed. This process is also suitable for other thermosetting phenolic resin, melamine resin, and epoxy resin membrane filtration material preparation, thus greatly expanding the ultrafiltration membrane raw material fields and scope.

2. Materials and Methods

2.1. Materials

Filter paper (100 g/m²) was obtained from Quzhou Kaile Co. Ltd., Quzhou, China. Urea-formaldehyde resin (43 wt%) was obtained from Langfang Senbang Co. Ltd., Langfang, China. Hydrochloric acid (37 wt%), sodium carboxymethylcellulose, and anhydrous alcohol were purchased from Nanjing Chemical Regent Co. Ltd., Nanjing, China. All chemicals were used as received without further purification.

2.2. Preparation of the Composite Membranes

Solid sodium carboxymethylcellulose (CMC) was wetted by a small amount of anhydrous alcohol. Then, a 1 wt% CMC solution was obtained by dissolving CMC in distilled water and stirring for 4 h at 60 °C. The obtained solution was maintained at room temperature for 24 h. Then, a set concentration of UFR was prepared, followed by the addition of a set amount of CMC and hydrochloric acid into the UFR solution with mechanical stirring at 55 °C. The mixed UFR solution was further treated with a sonicator (Q125, Qsonica, New York, NY, USA) for 10 min to remove bubbles.

A bar-coating method was employed to coat the as-prepared mixture coating solution onto the filter paper [45]. First, the paper was fixed on a glass plate and 2 mL of coating solution was added to the paper. Next, the solution was coated on the papers by wiping with a No. 20 coating rod (SG80QZ, RK PrintCoat Instruments Ltd., Royston, UK). The coated filter paper was placed in a drying oven for heat treatment. The composite ultrafiltration membrane was prepared successfully by the gelation-solidification of UFR.

2.3. Determination of Porosity

Membrane samples were placed in the drying oven at 105 °C for 5 h before measuring the dry weight (m_1). The membrane maintained in ethanol for 12 h was weighed (m_2) after removing superficial ethanol solution with filter paper. From the two weights (dry sample weight and wet sample weight), the porosity of membrane can be calculated according to Equation (1). Porosity is defined as:

$$P_r = \frac{m_2 - m_1}{V \times \rho} \times 100\% \quad (1)$$

Porosity is the percentage of the volume of open pores to the total volume. In the equation, P_r (%) is the porosity of the membrane, m_1 (g) is the bone dry weight of the membrane, m_2 (g) is the wet membrane weight after adsorption of ethanol, V (m³) is the volume of the membrane ($V = A \times l$, where A is the area of the membrane and l is the thickness of the membrane), and ρ is the density of ethanol (0.79 g/mL).

2.4. Determination of Pure Water Flux

This experiment was conducted using the standard pure water permeation detection method [46,47]. The prepared composite membrane was cut into an appropriate size and placed in an ultrafiltration cup. The composite membrane flux was determined by measuring the permeate volume under an operation pressure of 0.1 MPa at 25 °C. The water flux J_w (L/(m²·h)) was calculated using the Equation (2):

$$J_w = \frac{V}{A \Delta t} \quad (2)$$

where V (L) is the volume of permeated water, A (m²) is the membrane area, and Δt (h) is the permeation time.

2.5. Determination of Rejection Ratio

The rejection ratio was measured by filtrating bovine serum albumin solution (BSA, in 0.15 mol/L of NaCl buffered solution). The rejection can be calculated using the turbidimetric method [48,49]. After 30 min of filtration, the BSA concentrations in the feed solution and permeation solution were measured. The rejection ratio was calculated using Equation (3):

$$R = \frac{C_f - C_p}{C_f} \times 100\% \quad (3)$$

where C_p is the BSA concentration (g·L⁻¹) of the permeation solution and C_f is the initial BSA concentration (g·L⁻¹). The concentrations of the initial and permeation solution were analyzed on a UV-vis spectrophotometer (Evolution 201, Thermo Scientific, Waltham, MA, USA) with adsorption at 280 nm [50].

2.6. Morphological Study Methods

The morphology and structure of the composite membranes were observed by taking scanning electron microscope (SEM) images from the top surface and cross-section of the membrane samples. The membrane sample was immersed in liquid nitrogen for quick-freezing to obtain the cross-section morphology. All samples were freeze-dried and sputtered with gold prior to detection. The membranes were examined by field emission scanning electron microscopes (FE-SEM, JSM-7600F, JEOL, Tokyo, Japan). The pore size distribution of the membrane was determined by a specific surface area and pore structure analyzer (V-Sorb 2800P, GAPP, Beijing, China).

3. Results and Discussion

3.1. Preparation of Paper-Based UFR/CMC Composite Ultrafiltration Membrane and Its Formation Mechanism

Figure 1a shows a schematic of our strategy for the preparation of this composite ultrafiltration membrane. First, we introduce UFR to cellulose filter paper by a coating method. To control the gelation process of UFR and to make up for the defects of large pores in the membrane, a thickening agent was added to the system. Thickeners are generally water-soluble macromolecules, whose long chain structures facilitate the crosslinking reaction. CMC is a good dispersant and film-forming agent. Because of its superior water-retaining performance, CMC is also conducive to improving the porosity of the membrane. Therefore, CMC was selected as the thickener for the composite membrane. The addition of thickener will moderately block contact between the adhesive molecules and the acid solution, causing the film-forming liquid to slowly gel. The increased viscosity also has a good effect on the uniformity of the pore size.

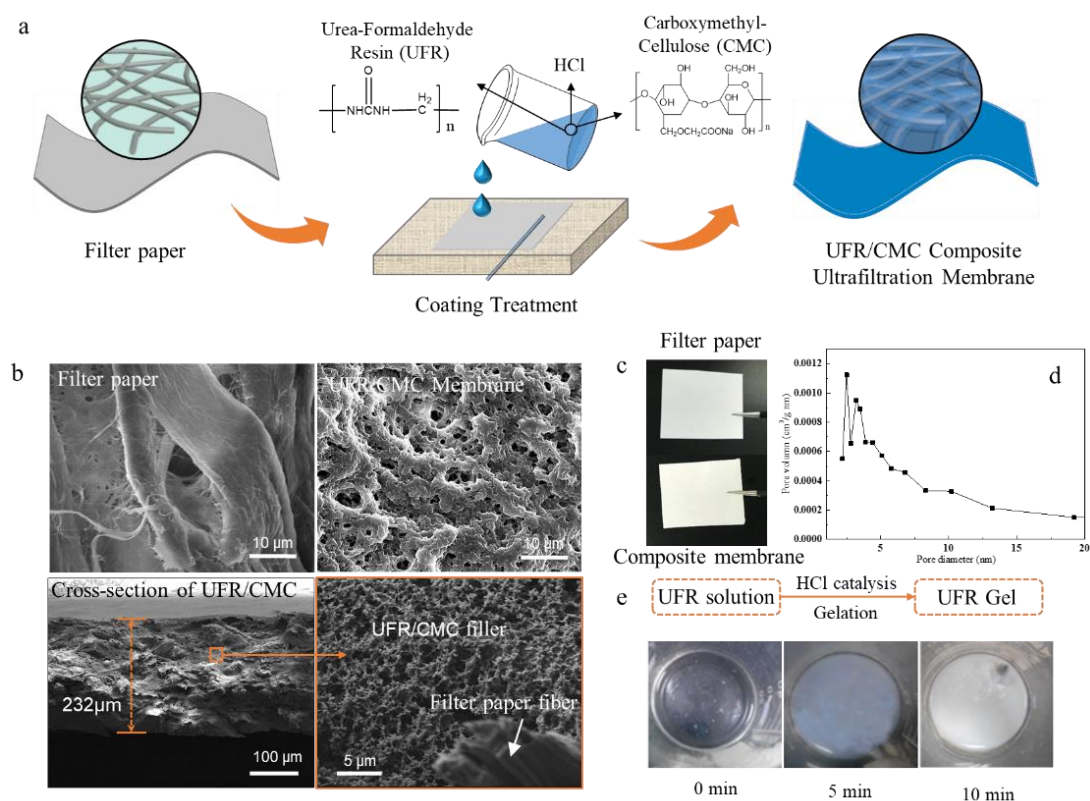


Figure 1. (a) Schematic illustration of preparation of the UFR/CMC composite ultrafiltration membrane (b) morphological images of the UFR/CMC composite ultrafiltration membrane (c) photos of filter paper and the composite ultrafiltration membrane (d) pore diameter distribution of the composite ultrafiltration membrane (e) changes in UFR gel degree over time with the addition of hydrochloric acid.

The morphology of the composite membrane top surface and cross-section was observed using FE-SEM, as shown in Figure 1b. During the fabrication process, resin fills the pores of the cellulose fiber network and cover the fiber surfaces. The results show that a porous resin layer with a thickness of $232 \pm 4 \mu\text{m}$ was formed on porous filter paper. Compared with the raw filter paper, more narrow pores, which may help to retain BSA, were formed on the surface of the coated filter paper. The composite membrane cross-sections showed a typical asymmetric morphology, including dense small-pore structures in the membrane.

Nitrogen adsorption was used to estimate the pore size distribution of the membrane. As shown in Figure 1d, the membrane has a bimodal peak distribution below 10 nm, which suggests the presence

of mesopores. The pore size distribution result is in good agreement with that of FE-SEM. It was concluded that the composite membrane fabricated in this project could be considered to be an ultrafiltration membrane.

As shown in Figure 1e, after adding hydrochloric acid to the aqueous solution of UFR, the resin undergoes a slow gelation process. Cured resins with different porosities can be obtained by controlling the speed of the gelation. We found that the gelation rate of UFR is slow without heating treatment. The efficiency of membrane production is low. In this case, heating treatment could shorten the gelation process of UFR. After optimization experiments, 55 °C was chosen as the heating temperature for UFR. Without the addition of thickening agent, the gelation of the resin was not uniform. The probability of macroporous defects in the prepared composite membrane was very high. The addition of CMC has positive effects on the production of a uniform porous resin ultrafiltration membrane.

3.2. Effects of CMC Content and UFR Concentration on the Performance of the Composite Membrane

In this experiment, urea-formaldehyde resin (UFR) solution with a concentration of 30% was prepared, and 0%, 5%, 10%, 15%, 20%, 25%, or 30% CMC (1 wt%) relative to the resin content was added to the solution. Then, hydrochloric acid (12 wt%) was used as a curing agent. Different composite membranes were prepared according to the amount of CMC added. The performance test results for the composite membrane are shown in Figure 2a. The addition of CMC to the resin membrane induced a decrease in water flux in comparison with that of the pure resin membrane: the water flux decreased with increasing CMC contents in the range of 0–30%. When the amount of CMC reached 30%, the water flux of the composite membrane was 400 L/(m²·h). However, the composite membrane showed a higher rejection ratio with the addition of CMC in comparison with that of the pure resin membrane. The rejection ratio increased from 52% to 92% with increasing CMC contents in the range of 0–30%. This can be explained as follows: the addition of CMC can result in the formation of a dense skin layer, thus providing fewer water transport pathways to limit water flux. CMC can also make the network structure denser, resulting in an increase in the rejection rate.

UFR aqueous solutions with concentrations of 10%, 15%, 20%, 25%, 30%, 35%, 40%, 45%, and 50% were prepared. Membrane solutions were prepared by mixing 20% CMC and hydrochloric acid (12 wt%) with the resin aqueous solution. Figure 2b shows the water flux and rejection ratio of the prepared composite membrane with different UFR concentrations. The pure water flux of the composite film decreased rapidly with an increase in resin concentration. When the UFR concentration reached 50%, the pure water flux of the composite membrane approached 470 L/(m²·h). It is obvious that the rejection ratio increased from 30% to 92% with an increase in resin concentration in the range of 10–50%. This can be explained as follows. A higher resin concentration can result in dense crosslinking, thus providing fewer water transport pathways and limiting water flux. A higher resin concentration can also make the network structure denser, resulting in an increase in the rejection ratio. Considering the application of the composite membrane, a resin concentration of 30% was selected for further experiments. With this concentration, the pure water flux of the composite membrane is approximately 800 L/(m²·h), and the rejection ratio is approximately 90%.

3.3. Effects of Acid on the Performance of the Composite Membrane

The gelation time of the composite ultrafiltration membrane prepared with different amounts of hydrochloric acid as curing agent is shown in Figure 3.

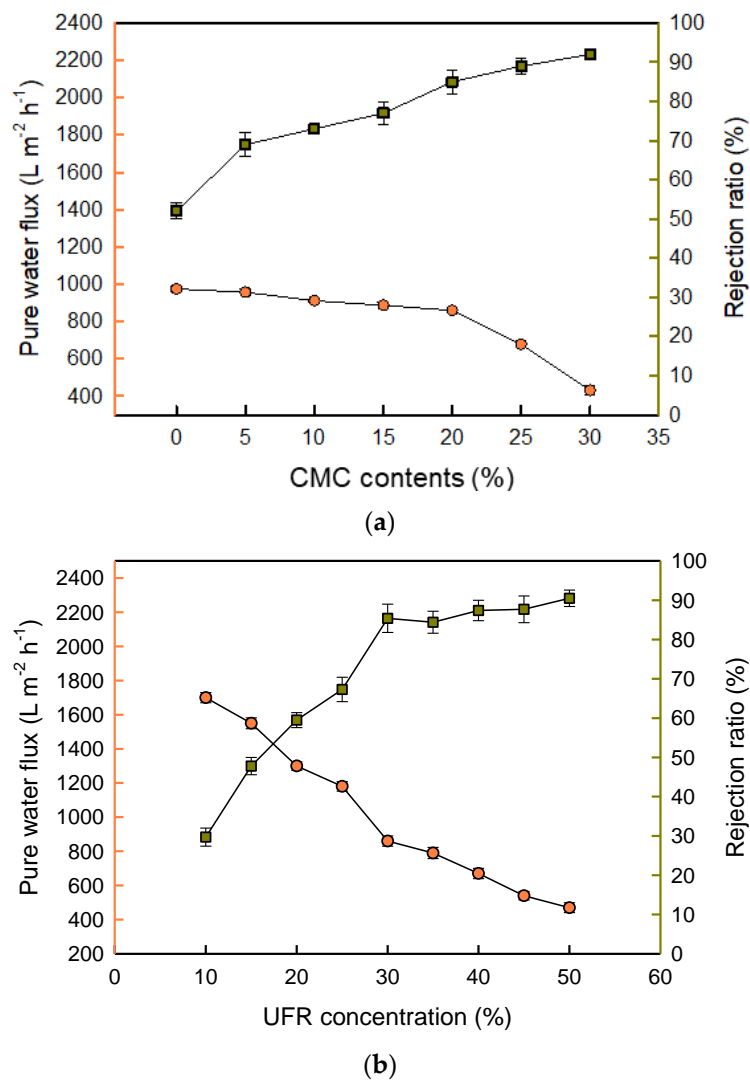


Figure 2. Effects of (a) CMC content and (b) urea-formaldehyde resin concentration on the pure water flux and rejection ratio of the composite membrane.

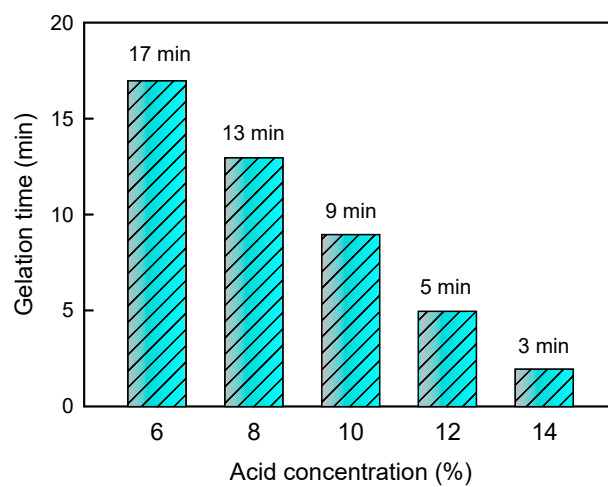


Figure 3. Effect of hydrochloric acid concentration on the gelation time of the composite membrane.

The gelation time of the composite ultrafiltration membrane prepared with different amounts of hydrochloric acid as curing agent is shown in Figure 3. The gelation time decreased with increasing hydrochloric acid concentration in the range of 6% to 14%. When the hydrochloric acid concentration is low, the gelation time of the resin is long. The increase in acid concentration in the resin membrane induces less water flux and a higher rejection ratio. This can be explained as follows. A small amount of acid is not enough to solidify the resin completely, resulting in a sparse network structure and poor rejection rate. If the concentration of hydrochloric acid is high, the resin gelation speed is too fast to control. Therefore, the ideal concentration of hydrochloric acid for fabrication of the composite membrane based on the comprehensive consideration of the pure water flux and rejection ratio is 12%, as shown in Figure 4a.

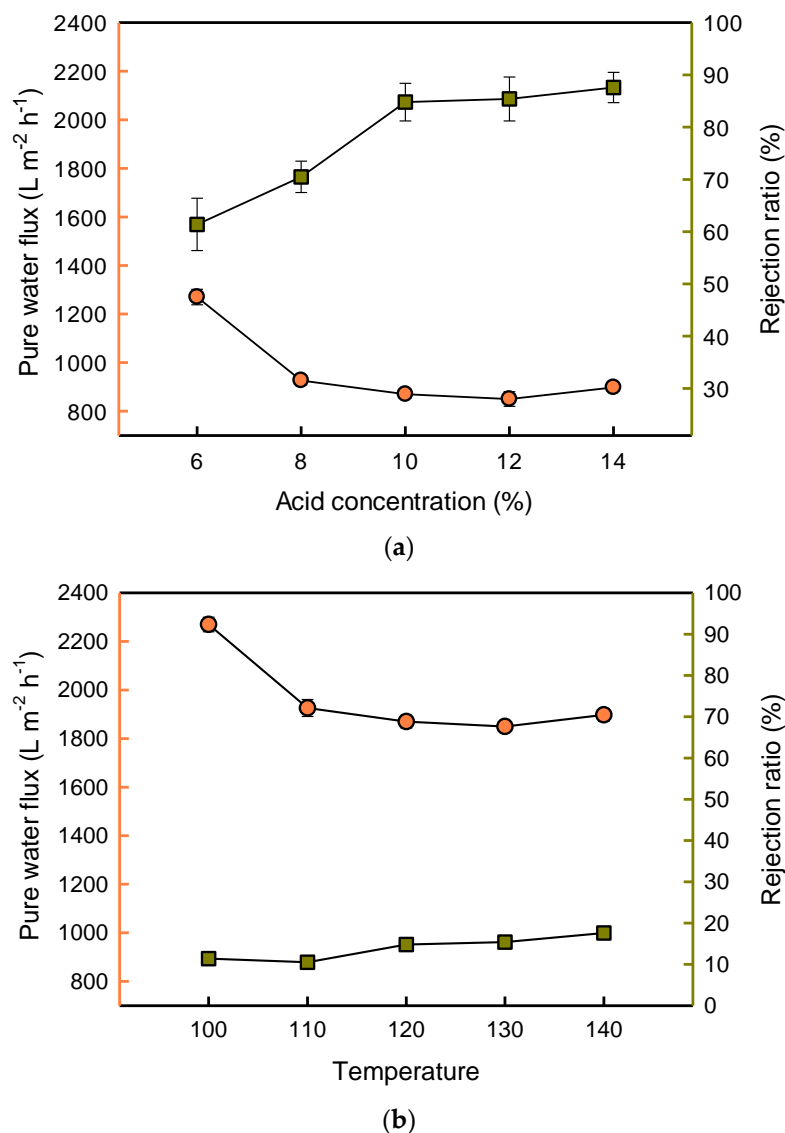


Figure 4. Pure water flux and rejection ratio of the composite membrane by acid-curing and heat-curing, respectively (a) Effect of hydrochloric acid concentration on the membrane performance (b) Effect of temperature on the membrane performance.

Figure 4b shows the effect of temperature on the permeability and rejection ratio of UFR composite membranes prepared by heat curing. The composite membrane prepared at 100 °C has a porosity ratio of 14.7%, a pure water flux of 2270 L/(m²·h), and a rejection ratio of 11.4% for bovine serum albumin (BSA). With an increase in temperature, the water flux is slightly decreased and the rejection ratio

shows an inverse tendency. A water flux of 1898 L/(m²·h) and rejection ratio of 17.6% were achieved when the temperature was increased to 140 °C. Because water evaporates easily at high temperatures, the porosity and rejection ratio of the composite membrane are maintained at a low level. The resin itself cross-links and solidifies, leading to a decrease in porosity. Furthermore, because of the excessive evaporation of water in the process of heat-curing, the membrane layer is brittle and easy to crack under high pressure, resulting in a large pure water flux and small rejection ratio.

3.4. Effect of Coating Weight on the Membrane

The optimal ratio was selected to prepare the membrane solution, the dosage was controlled, and the resin membrane layer was coated on the surface of the paper. Different composite membranes were prepared with different amounts of coating. The pure water flux and the rejection performance of BSA solution were tested. Figure 5 shows that the amount of resin used for the membrane influences the rejection performance of the membrane significantly. As the coating weight increased, the thickness of the film also increased. A denser membrane layer can result in a higher rejection ratio and less water flux. Controlling the appropriate amount of coating is essential for improving the membrane performance and controlling costs.

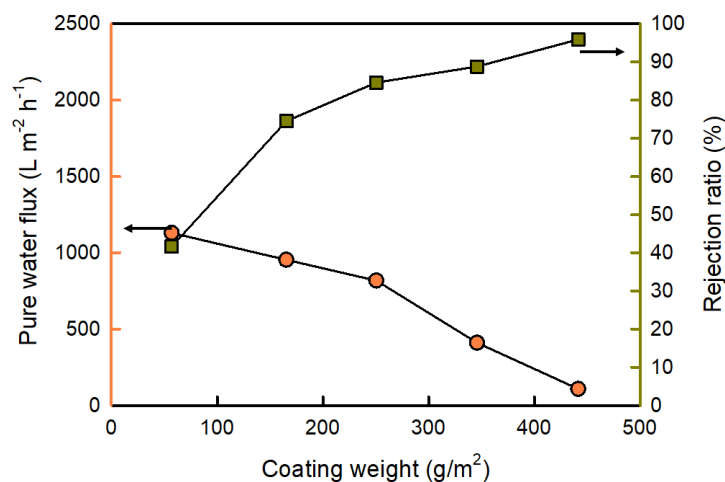


Figure 5. Effects of coating weight on the pure water flux and rejection ratio of the composite membrane.

3.5. Comparison of the Prepared Membranes with Those in the Literature

A comparison of the water flux and rejection ratio for our composite membrane with ultrafiltration membranes from the literature is shown in Table 1. In general, the UFR composite membrane shows a higher water flux than other UF membranes, with a desirable rejection ratio for BSA. It indicates clearly that the UFR can be suitable for potential use in wastewater treatment.

Table 1. Comparative water flux and rejection ratio of composite membranes.

Membrane	Water Flux (L/m ² ·h)	Rejection (%)	Reference
PVDF/GO	243	77.2	[51]
PVDF/PFSA	460	87.7	[52]
PVDF/PFSA	587	93.9	[52]
PAN-PF127	391	95	[53]
PAN-SiO ₂	234.3	99.3	[54]
PES-CA	63.3	84.6	[55]
PES-CA-Ag ₂ O	92.88	88.8	[55]
UFR	850	85	This work

4. Conclusions

This is the first time that a UFR-based ultrafiltration membrane was prepared successfully. In this research, filter paper was used as a template, water-soluble UFR was used as a precursor, a UFR solution was gelation-cured by adding hydrochloric acid. The addition of thickener can help make the pore size of the membrane uniform. The membrane property of the composite membrane prepared by acid-curing is much better than that prepared by heat-curing. The paper composite ultrafiltration membrane prepared under optimal conditions (UFR concentration of 30%, CMC dosage of 20% (resin dry), hydrochloric acid concentration of 12%, heating temperature of 55 °C, approximately 250 g/m² of coating) exhibited a rejection ratio of 85% and a pure water flux of 850 L/(m²·h).

Author Contributions: Conceptualization, Methodology, Validation, Resources, Data Curation, Writing—Original Draft Preparation, H.L.; Formal Analysis, Y.S. and L.Z.; Writing—Review and Editing, J.M. and X.Z.; Visualization, J.M.; Supervision, X.Z.; Project Administration, Funding Acquisition, X.Z. All authors have read and agreed to the published version of the manuscript.

Funding: This research was funded by the National Natural Science Foundation of China (Grant No. 31570576), the Natural Science Foundation of Jiangsu Provincial University (Grant No. 16KJA220005), the Doctorate Fellowship Foundation of Nanjing Forestry University, and the Priority Academic Program Development (PAPD) of Jiangsu Higher Education Institutions.

Acknowledgments: The authors acknowledge Analysis and Testing Center (Nanjing Forestry University) for the characterization of samples in this project.

Conflicts of Interest: The authors declare no conflict of interest.

References

1. Yong, M.; Zhang, Y.; Sun, S.; Liu, W. Properties of polyvinyl chloride (PVC) ultrafiltration membrane improved by lignin: Hydrophilicity and antifouling. *J. Membr. Sci.* **2019**, *575*, 50–59. [[CrossRef](#)]
2. Huang, H.; Schwab, K.; Jacangelo, J.G. Pretreatment for Low Pressure Membranes in Water Treatment: A Review. *Environ. Sci. Technol.* **2009**, *43*, 3011–3019. [[CrossRef](#)] [[PubMed](#)]
3. He, Z.; Ng, T.C.A.; Lyu, Z.; Gu, Q.; Zhang, L.; Ng, H.Y.; Wang, J. Alumina double-layered ultrafiltration membranes with enhanced water flux. *Colloids Surf. A Physicochem. Eng. Asp.* **2020**, *587*, 124324. [[CrossRef](#)]
4. Shi, Q.; Su, Y.; Zhu, S.; Li, C.; Zhao, Y.; Jiang, Z. A facile method for synthesis of pegylated polyethersulfone and its application in fabrication of antifouling ultrafiltration membrane. *J. Membr. Sci.* **2007**, *303*, 204–212. [[CrossRef](#)]
5. Jana, S.; Saikia, A.; Purkait, M.K.; Mohanty, K. Chitosan based ceramic ultrafiltration membrane: Preparation, characterization and application to remove Hg(II) and As(III) using polymer enhanced ultrafiltration. *Chem. Eng. J.* **2011**, *170*, 209–219. [[CrossRef](#)]
6. Sun, Z.; Chen, H.; Ren, X.; Zhang, Z.; Guo, L.; Zhang, F.; Cheng, H. Preparation and application of zinc oxide/poly(m-phenylene isophthalamide) hybrid ultrafiltration membranes. *J. Appl. Polym. Sci.* **2019**, *136*, 47583. [[CrossRef](#)]
7. Chen, W.; Peng, J.; Su, Y.; Zheng, L.; Wang, L.; Jiang, Z. Separation of oil/water emulsion using Pluronic F127 modified polyethersulfone ultrafiltration membranes. *Sep. Purif. Technol.* **2009**, *66*, 591–597. [[CrossRef](#)]
8. Qiu, Z.; Ji, X.; He, C. Fabrication of a loose nanofiltration candidate from Polyacrylonitrile/Graphene oxide hybrid membrane via thermally induced phase separation. *J. Hazard. Mater.* **2018**, *360*, 122–131. [[CrossRef](#)]
9. He, X.; Chen, C.; Jiang, Z.; Su, Y. Computer simulation of formation of polymeric ultrafiltration membrane via immersion precipitation. *J. Membr. Sci.* **2011**, *371*, 108–116. [[CrossRef](#)]
10. Altinkaya, S. Modeling of asymmetric membrane formation by dry-casting method. *J. Membr. Sci.* **2004**, *230*, 71–89. [[CrossRef](#)]
11. Dehban, A.; Kargari, A.; Zokaee Ashtiani, F. Preparation and characterization of an antifouling poly (phenyl sulfone) ultrafiltration membrane by vapor-induced phase separation technique. *Sep. Purif. Technol.* **2019**, *212*, 986–1000. [[CrossRef](#)]
12. Zhang, X.; Chen, Y.; Konsowa, A.H.; Zhu, X.; Crittenden, J.C. Evaluation of an innovative polyvinyl chloride (PVC) ultrafiltration membrane for wastewater treatment. *Sep. Purif. Technol.* **2009**, *70*, 71–78. [[CrossRef](#)]

13. Mahanty, B.; Satpati, A.K.; Kumar, S.; Leoncini, A.; Huskens, J.; Verboom, W.; Mohapatra, P.K. Development of polyvinyl chloride (PVC)-based highly efficient potentiometric sensors containing two benzene-centered tripodal diglycolamides as ionophores. *Sens. Actuators B Chem.* **2020**, *318*, 127961. [[CrossRef](#)]
14. Freger, V. Nanoscale Heterogeneity of Polyamide Membranes Formed by Interfacial Polymerization. *Langmuir* **2003**, *19*, 4791–4797. [[CrossRef](#)]
15. Paseto, L.; Luque-Alled, J.M.; Malankowska, M.; Navarro, M.; Gorgojo, P.; Coronas, J.; Téllez, C. Functionalized graphene-based polyamide thin film nanocomposite membranes for organic solvent nanofiltration. *Sep. Purif. Technol.* **2020**, *247*, 116995. [[CrossRef](#)]
16. Kaur, H.; Bulasara, V.K.; Gupta, R.K. Influence of pH and temperature of dip-coating solution on the properties of cellulose acetate-ceramic composite membrane for ultrafiltration. *Carbohydr. Polym.* **2018**, *195*, 613–621. [[CrossRef](#)] [[PubMed](#)]
17. Zavastin, D.; Cretescu, I.; Bezdadea, M.; Bourceanu, M.; Drăgan, M.; Lisa, G.; Mangalagiu, I.; Vasić, V.; Savić, J. Preparation, characterization and applicability of cellulose acetate–polyurethane blend membrane in separation techniques. *Colloids Surf. A Physicochem. Eng. Asp.* **2010**, *370*, 120–128. [[CrossRef](#)]
18. Yan, S.; Song, W.; Lu, J.; Wang, J.; Zheng, Y.; Xiao, R. Post-fabrication modifications of thermoplastic polymeric nanofiber membranes with electroactive polymers for triboelectric nanogenerators. *Nano Energy* **2019**, *59*, 697–704. [[CrossRef](#)]
19. Shao, J.; Qin, S.; Davidson, J.; Li, W.; He, Y.; Zhou, H.S. Recovery of nickel from aqueous solutions by complexation-ultrafiltration process with sodium polyacrylate and polyethylenimine. *J. Hazard. Mater.* **2013**, *244*, 472–477. [[CrossRef](#)]
20. Ouni, H.; Dhahbi, M. Spectrometric study of crystal violet in presence of polyacrylic acid and polyethylenimine and its removal by polyelectrolyte enhanced ultrafiltration. *Sep. Purif. Technol.* **2010**, *72*, 340–346. [[CrossRef](#)]
21. Mbareck, C.; Nguyen, Q.T.; Alaoui, O.T.; Barillier, D. Elaboration, characterization and application of polysulfone and polyacrylic acid blends as ultrafiltration membranes for removal of some heavy metals from water. *J. Hazard. Mater.* **2009**, *171*, 93–101. [[PubMed](#)]
22. Cheng, H.; Lan, J.-F.; Wei, G.-H.; Huang, W.-H.; Cheng, J.-K. Study on antifouling performance of single-walled carbon nanotubes modified electrode and its application in determination of 5-hydroxytryptamine. *Chin. J. Anal. Chem.* **2013**, *41*, 540. [[CrossRef](#)]
23. Luo, M.-L.; Zhao, J.-Q.; Tang, W.; Pu, C.-S. Hydrophilic modification of poly(ether sulfone) ultrafiltration membrane surface by self-assembly of TiO₂ nanoparticles. *Appl. Surf. Sci.* **2005**, *249*, 76–84. [[CrossRef](#)]
24. Yan, L.; Li, Y.S.; Xiang, C.B.; Xianda, S. Effect of nano-sized Al₂O₃-particle addition on PVDF ultrafiltration membrane performance. *J. Membr. Sci.* **2006**, *276*, 162–167. [[CrossRef](#)]
25. Yu, H.; Zhang, X.; Zhang, Y.; Liu, J.; Zhang, H. Development of a hydrophilic PES ultrafiltration membrane containing SiO₂@N-Halamine nanoparticles with both organic antifouling and antibacterial properties. *Desalination* **2013**, *326*, 69–76. [[CrossRef](#)]
26. Yan, X.; Qian, X.; Chang, Y. Preparation and characterization of urea formaldehyde@epoxy resin microcapsule on waterborne wood coatings. *Coatings* **2019**, *9*, 475. [[CrossRef](#)]
27. Raquez, J.-M.; Deléglise, M.; Lacrampe, M.-F.; Krawczak, P. Thermosetting (bio)materials derived from renewable resources: A critical review. *Prog. Polym. Sci.* **2010**, *35*, 487–509. [[CrossRef](#)]
28. Gourichon, B.; Deléglise, M.; Binetruy, C.; Krawczak, P. Dynamic void content prediction during radial injection in liquid composite molding. *Compos. Part A Appl. Sci. Manuf.* **2008**, *39*, 46–55. [[CrossRef](#)]
29. Bliznakov, E.D.; White, C.C.; Shaw, M.T. Mechanical properties of blends of HDPE and recycled urea-formaldehyde resin. *J. Appl. Polym. Sci.* **2000**, *77*, 3220–3227. [[CrossRef](#)]
30. Park, B.-D.; Kang, E.C.; Park, J.Y. Effects of formaldehyde to urea mole ratio on thermal curing behavior of urea–formaldehyde resin and properties of particleboard. *J. Appl. Polym. Sci.* **2006**, *101*, 1787–1792. [[CrossRef](#)]
31. Soroko, I.; Bhole, Y.; Livingston, A.G. Environmentally friendly route for the preparation of solvent resistant polyimide nanofiltration membranes. *Green Chem.* **2011**, *13*, 162–168. [[CrossRef](#)]
32. Varanasi, S.; Low, Z.-X.; Batchelor, W. Cellulose nanofibre composite membranes–Biodegradable and recyclable UF membranes. *Chem. Eng. J.* **2015**, *265*, 138–146. [[CrossRef](#)]

33. Qin, J.-J.; Wong, F.-S.; Li, Y.; Liu, Y.-T. A high flux ultrafiltration membrane spun from PSU/PVP (K90)/DMF/1,2-propanediol. *J. Membr. Sci.* **2003**, *211*, 139–147. [[CrossRef](#)]
34. Zhao, S.; Yan, W.; Shi, M.; Wang, Z.; Wang, J.; Wang, S. Improving permeability and antifouling performance of polyethersulfone ultrafiltration membrane by incorporation of ZnO-DMF dispersion containing nano-ZnO and polyvinylpyrrolidone. *J. Membr. Sci.* **2015**, *478*, 105–116. [[CrossRef](#)]
35. Yue, X.; Li, J.; Zhang, T.; Qiu, F.; Yang, D.; Xue, M. In situ one-step fabrication of durable superhydrophobic-superoleophilic cellulose/LDH membrane with hierarchical structure for efficiency oil/water separation. *Chem. Eng. J.* **2017**, *328*, 117–123. [[CrossRef](#)]
36. Mohamed, M.A.; Salleh, W.N.W.; Jaafar, J.; Hir, Z.A.M.; Rosmi, M.S.; Mutalib, M.A.; Ismail, A.F.; Tanemura, M. Regenerated cellulose membrane as bio-template for in-situ growth of visible-light driven C-modified mesoporous titania. *Carbohydr. Polym.* **2016**, *146*, 166–173. [[CrossRef](#)] [[PubMed](#)]
37. Hu, M.-X.; Niu, H.-M.; Chen, X.-L.; Zhan, H.-B. Natural cellulose microfiltration membranes for oil/water nanoemulsions separation. *Colloids Surf. A Physicochem. Eng. Asp.* **2019**, *564*, 142–151. [[CrossRef](#)]
38. Madaeni, S.S.; Heidary, F. Improving separation capability of regenerated cellulose ultrafiltration membrane by surface modification. *Appl. Surf. Sci.* **2011**, *257*, 4870–4876. [[CrossRef](#)]
39. Rojo, E.; Peresin, M.S.; Sampson, W.W.; Hoeger, I.C.; Vartiainen, J.; Laine, J.; Rojas, O.J. Comprehensive elucidation of the effect of residual lignin on the physical, barrier, mechanical and surface properties of nanocellulose films. *Green Chem.* **2015**, *17*, 1853–1866. [[CrossRef](#)]
40. Khan, A.; Wen, Y.; Huq, T.; Ni, Y. Cellulosic nanomaterials in food and nutraceutical applications: A review. *J. Agric. Food Chem.* **2018**, *66*, 8–19. [[CrossRef](#)]
41. Lu, H.; Zhang, L.; Ma, J.; Alam, N.; Zhou, X.; Ni, Y. Nano-cellulose/MOF derived carbon doped CuO/Fe₃O₄ nanocomposite as high efficient catalyst for organic pollutant remedy. *Nanomaterials* **2019**, *9*, 277. [[CrossRef](#)]
42. Lu, H.; Zhang, L.; Wang, B.; Long, Y.; Zhang, M.; Ma, J.; Khan, A.; Chowdhury, S.P.; Zhou, X.; Ni, Y. Cellulose-supported magnetic Fe₃O₄-MOF composites for enhanced dye removal application. *Cellulose* **2019**, *26*, 4909–4920. [[CrossRef](#)]
43. Dai, L.; Long, Z.; Chen, J.; An, X.; Cheng, D.; Khan, A.; Ni, Y. Robust guar gum/cellulose nanofibrils multilayer films with good barrier properties. *ACS Appl. Mater. Interfaces* **2017**, *9*, 5477–5485. [[CrossRef](#)]
44. Wang, J.; Zhou, X.; Ma, J. Preparation and characteristics of a paper-based ultrafiltration membrane. *BioResources* **2012**, *7*, 0545–0553.
45. Jung, J.; Raghavendra, G.M.; Kim, D.; Seo, J. One-step synthesis of starch-silver nanoparticle solution and its application to antibacterial paper coating. *Int. J. Biol. Macromol.* **2018**, *107*, 2285–2290. [[CrossRef](#)]
46. Gao, Q.; Wang, C.-Z.; Liu, S.; Hanigan, D.; Liu, S.-T.; Zhao, H.-Z. Ultrafiltration membrane microreactor (MMR) for simultaneous removal of nitrate and phosphate from water. *Chem. Eng. J.* **2019**, *355*, 238–246. [[CrossRef](#)]
47. Ahmad, A.L.; Sarif, M.; Ismail, S. Development of an integrally skinned ultrafiltration membrane for wastewater treatment: Effect of different formulations of PSf/NMP/PVP on flux and rejection. *Desalination* **2005**, *179*, 257–263. [[CrossRef](#)]
48. Xu, Z.; Li, X.; Teng, K.; Zhou, B.; Ma, M.; Shan, M.; Jiao, K.; Qian, X.; Fan, J. High flux and rejection of hierarchical composite membranes based on carbon nanotube network and ultrathin electrospun nanofibrous layer for dye removal. *J. Membr. Sci.* **2017**, *535*, 94–102. [[CrossRef](#)]
49. Lianchao, L.; Baoguo, W.; Huimin, T.; Tianlu, C.; Jiping, X. A novel nanofiltration membrane prepared with PAMAM and TMC by in situ interfacial polymerization on PEK-C ultrafiltration membrane. *J. Membr. Sci.* **2006**, *269*, 84–93. [[CrossRef](#)]
50. Zhao, Z.; Zheng, J.; Wang, M.; Zhang, H.; Han, C.C. High performance ultrafiltration membrane based on modified chitosan coating and electrospun nanofibrous PVDF scaffolds. *J. Membr. Sci.* **2012**, *394*, 209–217. [[CrossRef](#)]
51. Li, M.; Li, H.; Fang, F.; Deng, X.; Ma, S. Astragaloside IV attenuates cognitive impairments induced by transient cerebral ischemia and reperfusion in mice via anti-inflammatory mechanisms. *Neurosci. Lett.* **2017**, *639*, 114–119. [[CrossRef](#)] [[PubMed](#)]
52. Liu, X.; Yuan, H.; Wang, C.; Zhang, S.; Zhang, L.; Liu, X.; Liu, F.; Zhu, X.; Rohani, S.; Ching, C.; et al. A novel PVDF/PFSA-g-GO ultrafiltration membrane with enhanced permeation and antifouling performances. *Sep. Purif. Technol.* **2020**, *233*, 116038. [[CrossRef](#)]

53. Beril Melbiah, J.S.; Kaleekkal, N.J.; Nithya Rabekkal, D.; Rana, D.; Nagendran, A.; Mohan, D. Improved permeation, separation and antifouling performance of customized polyacrylonitrile ultrafiltration membranes. *Chem. Eng. Res. Des.* **2020**, *159*, 157–169. [[CrossRef](#)]
54. Liu, Q.; Li, L.; Pan, Z.; Dong, Q.; Xu, N.; Wang, T. Inorganic nanoparticles incorporated in polyacrylonitrile-based mixed matrix membranes for hydrophilic, ultrafast, and fouling-resistant ultrafiltration. *J. Appl. Polym. Sci.* **2019**, *136*, 47902. [[CrossRef](#)]
55. Gul, S.; Rehan, Z.A.; Khan, S.A.; Akhtar, K.; Khan, M.A.; Khan, M.I.; Rashid, M.I.; Asiri, A.M.; Khan, S.B. Antibacterial PES-CA-Ag₂O nanocomposite supported Cu nanoparticles membrane toward ultrafiltration, BSA rejection and reduction of nitrophenol. *J. Mol. Liq.* **2017**, *230*, 616–624. [[CrossRef](#)]



© 2020 by the authors. Licensee MDPI, Basel, Switzerland. This article is an open access article distributed under the terms and conditions of the Creative Commons Attribution (CC BY) license (<http://creativecommons.org/licenses/by/4.0/>).